The Seismic Record
A journal of the Seismological Society of America

Razor-Sharp Edge—The Yakutat Slab Dissecting South-Central Alaska

Meghan S. Miller*[1], Ping Zhang[1], Robert Pickle[1], Trevor S. Waldien[2], and Sarah M. Roeske[3]

Abstract

The tectonics of south-central Alaska are dominated by subduction of the Pacific plate, the Yakutat oceanic plateau, and evolution of the major continental fault system, the Denali fault. Our new structural images show the razor-sharp edge and extent of the Yakutat slab as it subducts beneath the North American plate with remarkable detail. Thousands of small, previously undetected earthquakes form a prominent linear cluster that illuminates the precise edge of the subducted Yakutat microplate and defines the location of changing slab morphology reflecting the change in stress state. Our new seismic images and refined locations of down-dipping seismicity further elucidate the lack of mantle wedge below the Denali volcanic gap and the northeastern margin of the subducted Yakutat microplate, imaged here to be directly below the curved section of the Denali fault. We suggest these features have controlled the nucleation of the 2002 M_w 7.9 Denali fault earthquake and the position of recently onset volcanic fields.

Cite this article as Miller, M. S., P. Zhang, R. Pickle, T. S. Waldien, and S. M. Roeske (2026). Razor-Sharp Edge—The Yakutat Slab Dissecting South-Central Alaska, *The Seismic Record*. **6**(**2**), 230–238, doi: 10.1785/0320250055.

Supplemental Material

Introduction

The Denali fault is a right-lateral continental strike-slip fault that transects the North American Cordillera from northern British Columbia to the Bering Sea. The complexity of the fault system changes along strike, ranging from a multistranded fault in western Alaska to a well-defined locus of master faults in southwestern Yukon. In contrast, in central Alaska, the highly localized master strand, the Denali fault itself, is bordered by splay thrust systems that include the Susitna Glacier thrust fault (Fig. 1). The 3 November 2002 M_w 7.9 Denali fault earthquake initiated on the previously unknown Susitna glacier thrust fault (star in Fig. 1) and then transferred onto the main Denali fault and the Totschunda fault (Eberhart-Phillips *et al.*, 2003; Crone *et al.*, 2004). The 2002 Denali earthquake's complex large rupture demonstrated that in central Alaska, both thrust faults and the strike-slip Denali fault accommodate oblique convergence from the Alaska–Aleutian subduction zone. This kinematically linked fault system has accumulated greater than 480 km of Cenozoic strike-slip displacement estimated from reconstruction of a dissected metamorphic belt between south-central Alaska and Yukon Territory and is interpreted to have accumulated during oblique subduction along the Cordilleran margin (Waldien *et al.*, 2024).

Although in central Alaska the Denali fault is localized, the complex tectonics of the Alaska Range, Chugach, and St Elias Mountains and Wrangell volcanic arc are controlled by the motion of the Pacific plate as it subducts beneath the North American continent, together with the subduction of the Yakutat microplate (Plafker *et al.*, 1994). The influence of the Yakutat microplate in southern Alaska is a prime example of a "congested subduction zone," and therefore many previous studies have used both active and passive source seismic imaging

1. Research School of Earth Sciences, Australian National University, Canberra, Australia, https://orcid.org/0000-0001-5494-2296 (MSM); https://orcid.org/0000-0003-1425-3925 (PZ); https://orcid.org/0000-0002-8550-5256 (RP); 2. Department of Geology and Geological Engineering, South Dakota School of Mines and Technology, Rapid City, South Dakota, U.S.A., https://orcid.org/0000-0001-5753-161X (TSW); 3. Department of Earth and Planetary Sciences, University of California-Davis, Davis, California, U.S.A., https://orcid.org/0000-0002-0511-5865 (SMR)

*Corresponding author: meghan.miller@anu.edu.au

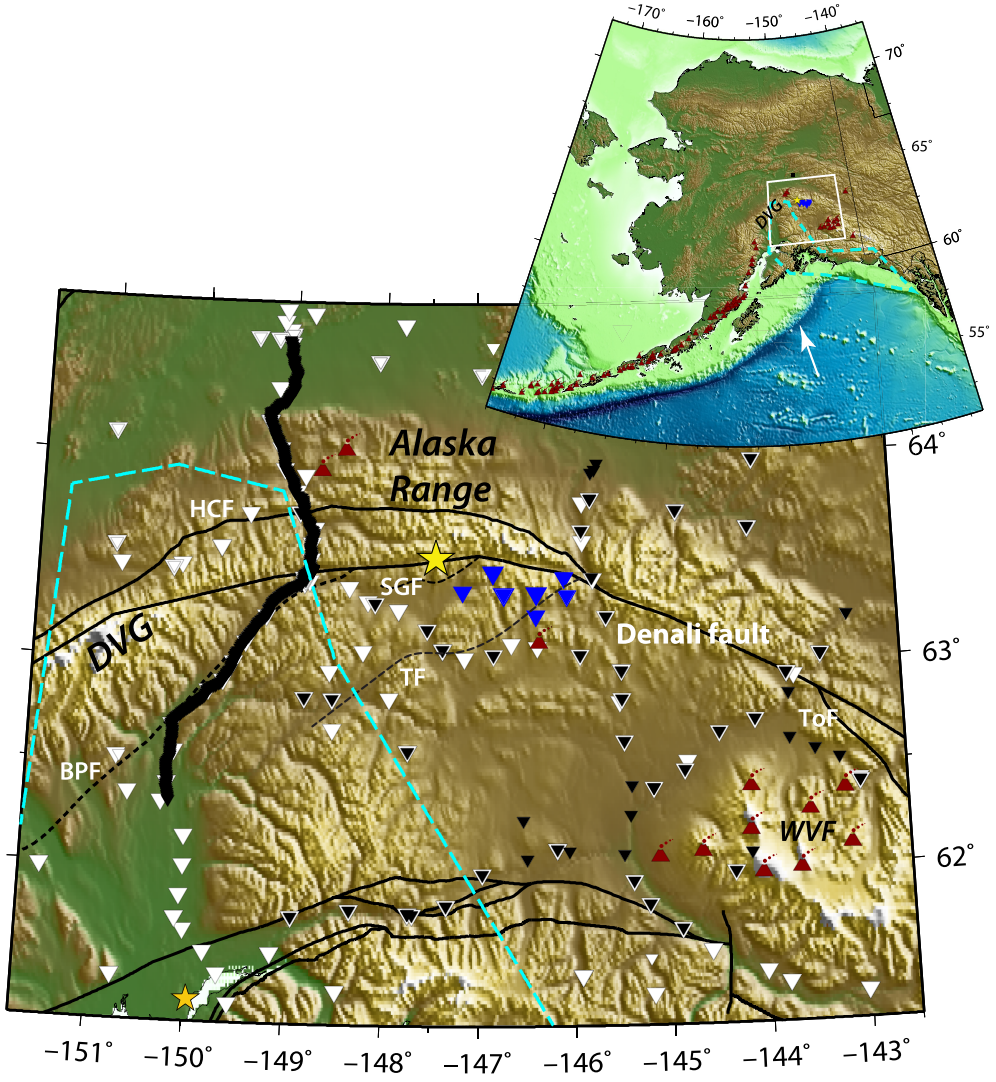

Figure 1. Shaded relief map of south-central Alaska and seismic stations. The black inverted triangles are the stations used for the seismicity catalog and ambient noise analyses, and the white inverted triangles are stations used for the *P* receiver functions. The stations in blue are the Z5 (ICED) network stations. Shaded topography is from ETOPO1 and the Quaternary volcanoes are indicated with dark red symbols from the Smithsonian volcano database. The yellow star indicates the epicenter of the 2002 M_w 7.9 Denali earthquake. The small orange star indicates the 2018 M_w 7.1 Anchorage earthquake epicenter. BPF, Broad Pass fault; DVG, Denali volcanic gap; HCF, Hines Creek fault; SGF, Susitna Glacier fault; TF, Talkeetna fault; ToF, Totschunda fault; WVF, Wrangel volcanic field. The dashed black lines are thrust faults. The inset shows the regional setting with blue triangles indicating the Z5 (ICED) network stations, and the interpreted position of the Yakutat plate (Eberhart-Phillips *et al.*, 2006) at depth as a cyan polygon and the vector indicates the Pacific-North America plate convergence direction.

techniques to define and track the position of the Yakutat microplate at depth, both onshore and offshore Alaska (Fuis *et al.*, 2008). Subduction of the Yakutat microplate has been identified as the source of many of the complexities in the tectonic observables, such as the lack of volcanism in the Denali volcanic gap (Worthington *et al.*, 2012), the lateral termination of Wadati–Benioff zone seismicity (Eberhart-Phillips *et al.*, 2006), position and longevity of the Wrangell volcanic arc (Brueseke *et al.*, 2019), and location of tectonic tremor (Wech, 2016), but its subducted extent and its morphology have been debated (Nye, 1999). Our new seismological observations and images, along with complementary geologic observations, document not only the position of the subducted Yakutat slab, but also that its inherent structural heterogeneities control the entire subduction zone system from mantle to the surface.

Methods

We used data recorded at stations shown with inverted triangles in Figure 1 to create a new machine learning (ML)-based earthquake catalog (Fig. 2), together with *P* receiver functions (PRFs) to image velocity discontinuities within the lithosphere (Fig. 3) and new images of the lithospheric structure from ambient noise tomography inferring the shear-wave velocities down to 50 km depth (Fig. 4). These stations were chosen as they are adjacent to the central section of the Denali fault and Alaska Range suture zone that has been under-resolved in previous imaging efforts.

Seismicity catalog

We utilized a modified version of the ML-based seismic phase picking package EQTransformer (Mousavi *et al.*, 2020), which is described in more detail in the supplemental material, available to this article, and used the AKAN2020 3D model (Nayak *et al.*,

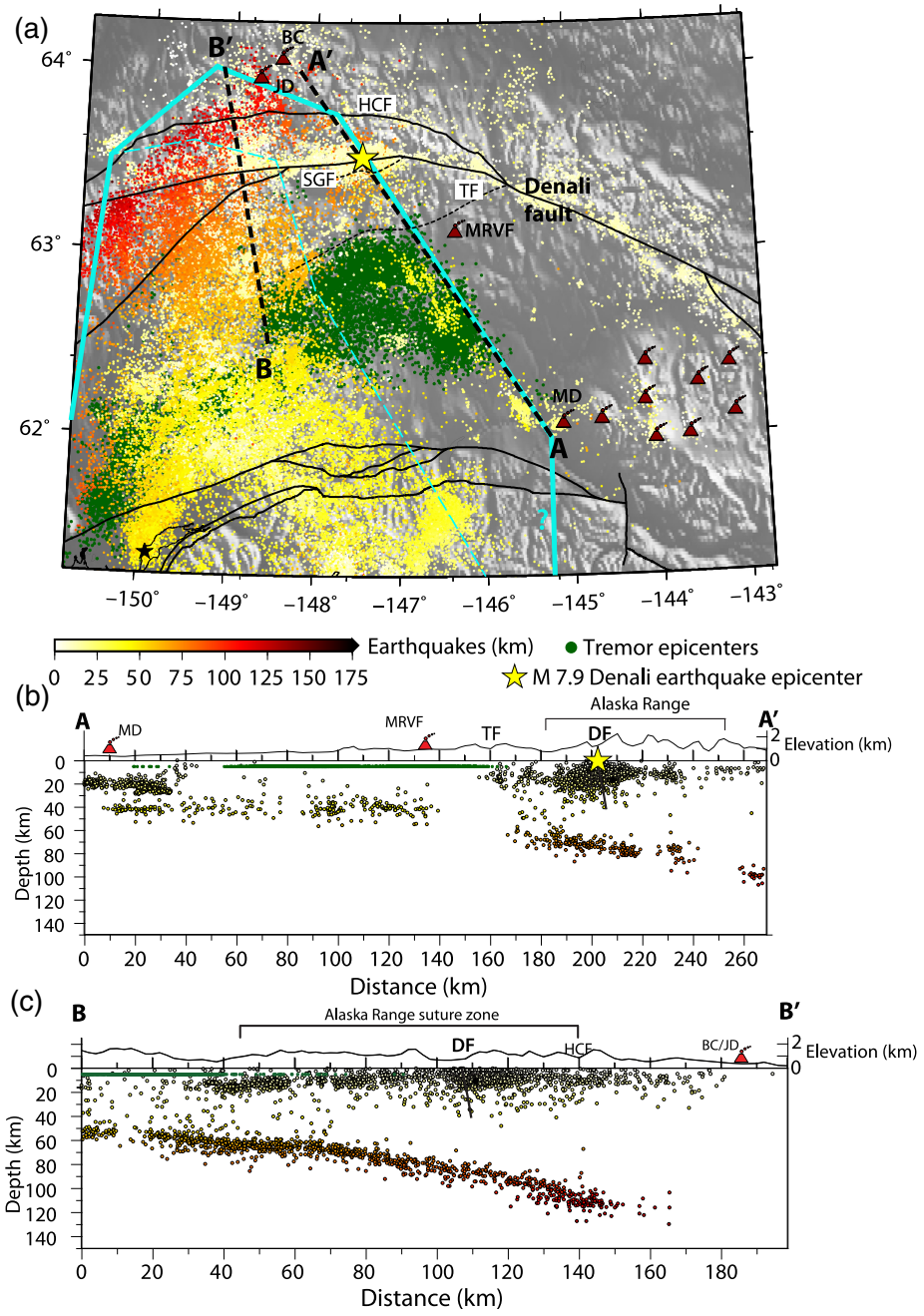

Figure 2. New machine learning (ML)-based catalog of seismicity occurring between 2018 and 2021, along with tectonic tremor (Wech, 2016). (a) Map of the earthquakes' hypocenters color-coded by depth. The cyan-dashed polygon represents the previously interpreted position of the Yakutat slab (Eberhart-Phillips *et al.*, 2006), and the solid cyan polygon represents the new inferred position of the Yakutat microplate at depth. The dark red volcano symbols represent the Quaternary volcanoes from the Smithsonian volcano database, with BC, Buzzard Creek; JD, Jumbo Dome; MD, Mt. Drum; and MRVF, Maclaren River volcanic field annotated. Faults modified from Colpron and Nelson (2020) are shown by black lines. DF, Denali fault; HCF, Hines Creek fault; SGF, Susitna Glacier fault; TF, Talkeetna fault. Locations of the profiles are indicated by the thick dashed lines A–A′ and B–B′. (b) Earthquake hypocenters 20 km on either side of the profile A–A′ are color-coded with depth as in Figure 2a and the tremor locations (Wech, 2016) as green dots at a fixed depth of 5 km for illustrative purposes. (c) As in Figure 2b above, but along profile B–B′. The small black star indicates the 2018 M_w 7.1 Anchorage earthquake epicenter.

2020) for NonLinLoc relocations. The data included 265 stations from the networks listed in Table S1 for the time period between 1 January 2018 and 20 December 2021. This duration was chosen to focus on the central Alaska Range suture zone and to best utilize the Z5 (2018) network. Events required at least seven total phase picks, with the number of $P > 2$, $S > 2$, and at least two stations having both a P and S phase pick. An example event and workflow are shown in Figure S1. Our final catalog was composed of 64,870 events from 1 January 2018 to 20 December 2021 with an average latitude, longitude, and depth uncertainty of 5.0, 5.2, and 8.6 km, respectively, an average root mean square (RMS) error of 0.38 s, and a mean of 18.4 P- and S-phase picks per event.

PRF analyses

PRFs were calculated with Funclab (Porritt and Miller, 2018). Three-component waveforms from earthquakes with magnitudes greater than **M** 6.0 at epicentral distances between 30° and 98° were used in the analysis for stations indicated with white inverted triangles in Figure 1. The receiver functions were calculated using an iterative time-domain deconvolution of the vertical component from the radial components about a 1 Hz central frequency within Funclab (Porritt and Miller, 2018). This workflow is

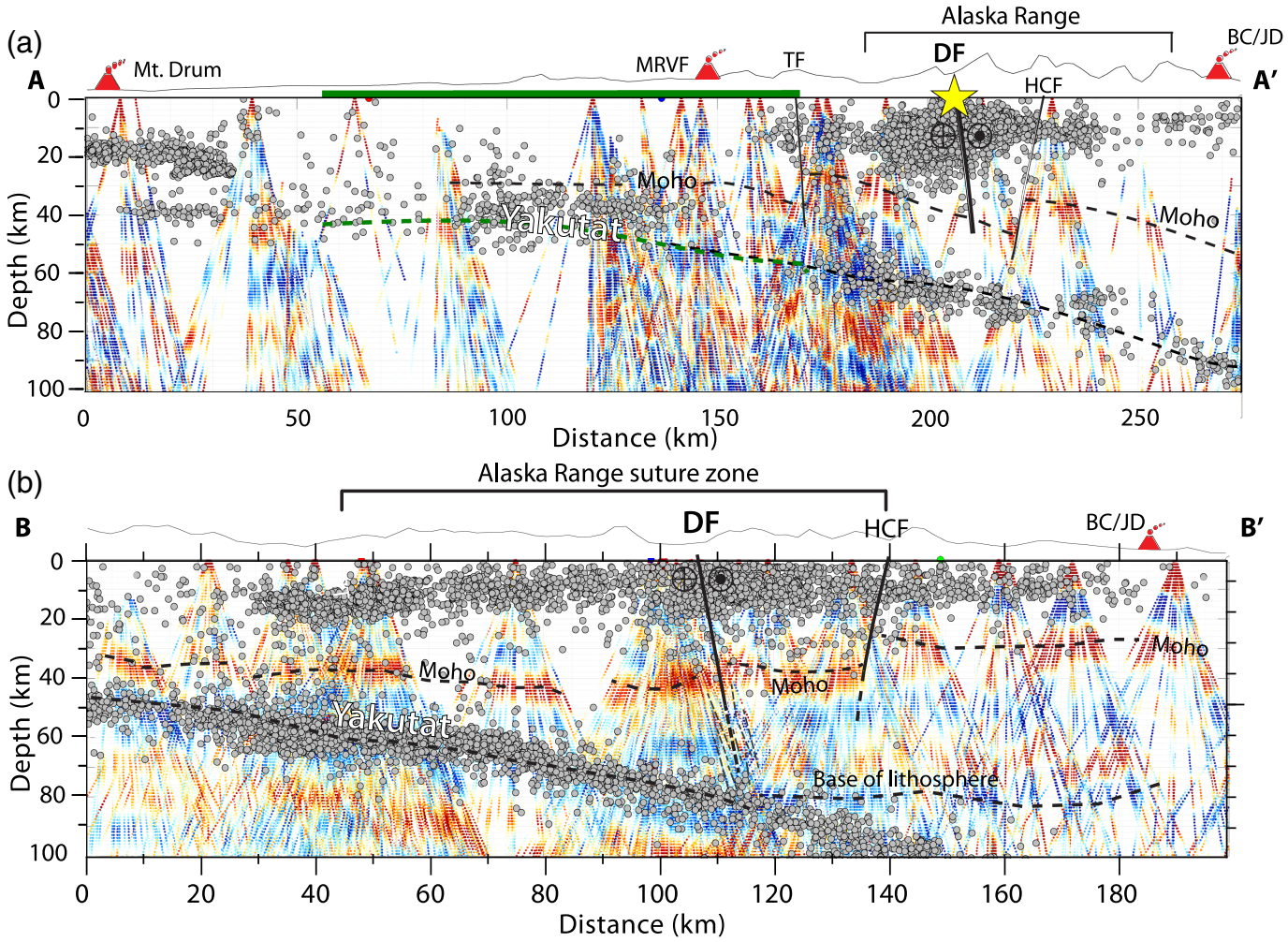

outlined in more detail in Miller *et al.* (2018) and in the supplemental material. Figure 3 and Figure S4 represent all receiver functions within 0.5° of the profiles shown in Figure 2a that are converted to depth using the 1D velocity model ak135 (Kennett *et al.*, 1995) and plotted along their individual ray paths.

Ambient noise tomography

We utilized SeisLib, an open-source Python package developed by Magrini *et al.* (2022) to process the vertical-component ambient noise data from 1 August 2017 to 1 August 2021. The simultaneous recordings among 23,005 station pairs were cross-correlated in the frequency domain for each time window and normalized by the spectral whitening. All cross-correlation functions (CCFs) were then stacked over their deployment periods, as shown in Figure S5. Then we measured the fundamental-mode Rayleigh-wave phase velocity dispersions up to 0.5 Hz based on the zero-crossings method, following Magrini *et al.* (2022) and described in more detail in the supplemental material. The measurements were quality-controlled with a minimum interstation path length of 1.5 wavelengths as a far-field approximation criterion, resulting in a final total of 5864 dispersions (Fig. S5) that were used in the inversion.

Figure 3. (a,b) Receiver function images of the lithospheric structure with seismicity and topography. Receiver functions (positive and negative amplitudes are shown as red and blue colors, respectively) along the profiles A–A′ and B–B′ (locations are shown in Fig. 2a) with the new ML-based seismicity catalog, where hypocenters are shown as gray dots and are projected within 20 km of the profile locations. BPF, Broad Pass fault; BC/JD, Buzzard Creek and Jumbo Dome volcanoes; DF, Denali fault; HCF, Hines Creek fault; MD, Mt. Drum volcano; MRVF, Maclaren River volcanic field; SGF, Susitna Glacier fault. The yellow star indicates the epicenter of the 2002 M_w 7.9 Denali earthquake. The green line on the surface is the projected extent of the tremor epicenters (Wech, 2016) as shown in Figure 2. The solid lines are interpretations based on geological observations, and the dashed lines are interpretations based on the receiver functions, and the green-dotted line is the projection of the tremor to the interpreted Yakutat–North American plate interface. The same profiles are shown in Figure S4 without earthquakes.

To constrain a 3D V_S model in the crust and uppermost mantle, we applied the 3D direct surface-wave inversion algorithm following Fang *et al.* (2015). It utilizes the fast-marching ray tracing method to calculate synthetic surface-wave travel times, at each period, and ray-paths station pairs, and subsequently inverts all data into a 3D V_S model directly (Fang *et al.*, 2015). The inverted model is set as 3 km layer thickness down to a depth of 50 km, with lateral grids of 0.15° in latitude and 0.35° in longitude, and is described in more detail in the supplemental material.

Results

Detailed seismicity patterns linked to the Yakutat plate

Seismicity patterns from the new ML-based catalog show a clear Wadati–Benioff zone from the subduction of the Pacific plate beneath the Denali Volcanic Gap and earthquakes occurring along the main strand of the Denali fault (Fig. 2), as expected. The catalog also locates the many (~35,000) crustal depth events (<35 km) throughout the region during 2018–2021. The aftershocks of the 30 November 2018 Anchorage earthquake (mainshock indicated by a black star in Fig. 2) are prominent in the southwestern region of the map and the alignment of upper crustal seismicity along the main strand of the Denali fault is clear from longitude −148° E to the Totschunda–Denali fault intersection at the eastern boundary of the map (Fig. 2a). There is also a clear cluster of events near Mt. Drum, the westernmost volcano in the Wrangell volcanic field (Fig. 2a), and to the northeast of that volcano. This cluster was coined the "Glennallen cluster" by Daly *et al.* (2021) and was interpreted to be related to the formation of a new volcano due to the crustal depth range.

However, the most prominent new pattern recognized here is the northwest–southeast (NW-SE)-striking alignment of earthquakes that are offset by approximately 1° laterally, yet parallel, from the main Wadati–Benioff zone that was partially defined by the eastern edge of the previously interpreted position of the subducted Yakutat plate (Eberhart-Phillips *et al.*, 2006) (Fig. 2a) and dips to the NW (Fig. 2a,b). This ~250 km long linear cluster contains ~1750 earthquakes located near the profile A–A′ and south of the Denali fault. To the best of our knowledge, this cluster has not yet been identified in other catalogs despite additional instruments from the USArray Transportable Array deployment and expansion of the Alaska seismic network in the Alaska Earthquake Center (AEC) catalog (Ruppert and West, 2019) or using other temporary deployments, such as the YG network near the cluster (Daly *et al.*, 2021), as shown in Figure S3. This cluster is low magnitude (1.5 ± 0.4 M_L) but of reasonable quality, with mean horizontal and vertical hypocenter uncertainties of 3.2 and 6.3 km, respectively, mean RMS error 0.40 ± 0.13 s, mean event phase and station count of 20.1 and 11.4, respectively, and a mean azimuthal gap of 129. Six total networks contributed to these events, with AK (46%) representing the majority of defining arrivals, followed by YG (30.5%), TA (11.5%), and AV, Z5, AT, and ZE all <5%. 50% of these events occurred in 2018, which may suggest time-correlated activity and/or station bias. To ensure these events were legitimate, we also plotted the arrivals of each and went through them manually, removing any mislocated teleseisms that were otherwise poorly defined. The trend of these NW-striking earthquakes (Fig. 2b) dips more shallowly than the Wadati–Benioff zone earthquakes farther to the west beneath the Denali volcanic gap (Fig. 2c) associated with the subduction of the Pacific plate. The abrupt lateral termination of these earthquakes around −145.5° E has a strike that is subparallel to the previously interpreted edge of the subducted Yakutat microplate, as indicated in Figure 2a (Eberhart-Phillips *et al.*, 2006). Even more curious is the correlation of these earthquakes with the northeast (NE) extent of the tectonic tremor epicenters identified by Wech (2016) (Fig. 2a–c). Wech (2016) interpreted the tremor locations to be semicontinuous slip on the interface of the Yakutat–North American plate interface, and as evidence, the megathrust extended farther than the Wadati–Benioff zone earthquakes indicate. Between where the Wadati–Benioff earthquakes decrease in number, near the previously interpreted subducted Yakutat plate (Eberhart-Phillips *et al.*, 2006) the deformation seems to be mostly accommodated by tremor (Wech, 2016) until the linear cluster of earthquakes appear (Fig. 2a). This newly identified linear trend of seismicity extends beyond the northern terminus of tremor, located near the surface expression of the Talkeetna fault (TF) with a dip to the NW to more than 120 km depth beneath the northern flank of the Alaska Range (Fig. 2b). The strike of this linear cluster also intersects a cluster of seismicity in the upper crust (<10 km depth) near the 2002 M_w 7.9 epicenter (Fig. 2a,b). To the east of this linear cluster, beneath the Copper River basin and the Wrangell volcanic field, there is a distinct lack of seismicity at all depths. The new ML seismicity catalog also illuminates the top of the Yakutat slab as it subducts beneath the central Alaska Range colocated with a strong negative seismic velocity signal (representing a velocity decrease with depth) that dips to the NE between 40 and 80 km depth as independently imaged

with PRFs (Fig. 3). The correlation of the strong negative (blue) phase in the PRFs and the dipping seismicity supports the interpretation of the subducted Yakutat extending as far east as profile A–A′ (Fig. 2a,c), although the temporary stations are sparsely located and far less dense than along profile B–B′. However, this interpretation is further supported by profile B–B′, where a strong, dipping negative anomaly is observed slightly deeper (50–90 km depth), which previously has been identified in other receiver function studies (Fig. 3b) (compare with Ferris *et al.*, 2003; Rondenay *et al.*, 2010; Miller *et al.*, 2018; Mann *et al.*, 2022). Rondenay *et al.* (2010) interpreted this signal at approximately 60 km depth as a layer of ponded melt at the base of the overriding plate rather than the lithosphere–asthenosphere boundary. Miller *et al.* (2018) tentatively interpreted it as the lithosphere–asthenosphere boundary from common conversion point receiver functions, noting that these conversions could easily be muted or misidentified with this imaging method. Ferris *et al.* (2003) interpreted this thick feature linked to the offshore extent (Worthington *et al.*, 2012) as a subducted exotic terrane, and Mann *et al.* (2022) went further to suggest this feature as a low-velocity layer atop the underthrust Yakutat crust and interpreted it to be indicative of the megathrust. However, the clear alignment of the refined locations of down-dipping seismicity with the dipping, negative polarity signal in the receiver functions demonstrated here illustrate that this disputed feature is indeed the seismogenic interface of the subducting Yakutat plate in contact with the North American lithosphere in the absence of an asthenospheric wedge (Fig. 3). The lack of mantle wedge is indicative of the Denali volcanic gap, but resumed volcanism since ~1 Ma within the volcanic gap suggests that the mantle wedge may be re-establishing as the slab geometry evolves (Chuang *et al.*, 2017).

Discussion

The dynamics of congested subduction zones, where exotic terranes, such as an oceanic plateau, are caught up in the subduction of oceanic lithosphere, have been investigated through the rock record (Brueseke *et al.*, 2023), active seismic imaging (e.g., Worthington *et al.*, 2012; Christeson *et al.*, 2013; and via numerical simulations Moresi *et al.* (2014). A critical feature of the southern Alaska congested subduction zone is the long-lived obliquity of relative plate motion before and during Yakutat plate subduction. This obliquity, combined with increased plate coupling, resulted in laterally migrating magmatic arcs (Regan *et al.*, 2021), disruption of sediment routing systems (Finzel *et al.*, 2015), and surface uplift associated with strike-slip faults, such as the Denali fault. Here, we document with previously unidentified detail the ongoing collision and associated subduction processes of the buoyant Yakutat terrane with the overriding North American plate. Along with the previously recognized modifications to the rock record, surface topography, and lithospheric structure, the ongoing seismic activity captured here demonstrates the kinematic and mechanical linkage of various structures involved in oblique subduction zone clogging observed on the human timescale.

Within the upper plate of the congested subduction system, two critical relationships can be gleaned from the linear trend of crustal earthquakes along profile A–A′: (1) the earthquakes contain the main shock and aftershocks from the 2002 M_w 7.9 Denali earthquake; and (2) that cluster of seismicity coincides with the apex of curvature of the Alaska Range and Denali fault (Fig. 2a). The curvature of the Alaska Range and Denali fault is a primary feature of the southern Alaska plate margin that formed during oblique arc-continent collision before subduction of the Yakutat microplate (Waldien *et al.*, 2024). Yet, this geometric feature has been argued to affect fault kinematics, spatial distribution of historic seismicity, and crustal stress field associated with the Denali fault system (e.g., Ratchkovski *et al.*, 2004; Vallage *et al.*, 2014). Because shallow subduction angles have been shown to impart upper plate compression by end loading (e.g., Axen *et al.*, 2018), we propose that the kinematic linkage of thrust and strike-slip faults observed in the curved section of the fault during the 2002 earthquake may be the combined result of upper plate end loading and Denali fault curvature. Considering the observation that the linear trend of crustal seismicity along the A–A′ profile includes the 2002 event, we suggest that the northeastern margin of the Yakutat microplate, imaged here to be directly below the curved section of the fault, influenced nucleation of the 2002 event. Moreover, the seismicity (Vallage *et al.*, 2014) and active faulting recording contractional deformation above the slab edge in the apex of curvature support the previously hypothesized notion that oblique subduction of the Yakutat microplate results in upper-plate deformation that tightens the curvature of the southern Alaskan plate boundary (Redfield *et al.*, 2007), suggesting that oroclinal bending may be an underrecognized signal of congested subduction systems.

The trend of the ~250 km long linear zone of seismicity and the eastern extent of the tremor epicenters also aligns with the edge of the prominent fast *S*-wave velocity zones in the lower crust imaged with ambient noise tomography (Fig. 4). We

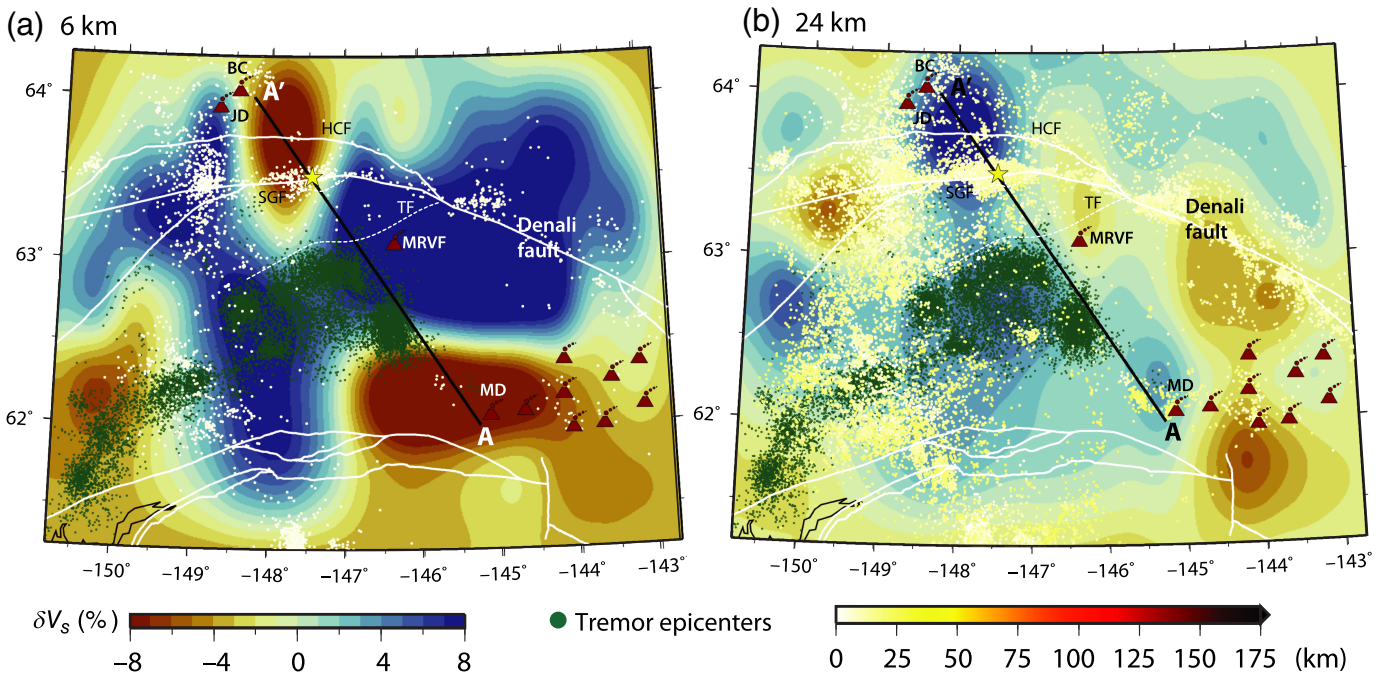

Figure 4. Shear-wave velocity model derived from ambient noise tomography at crustal depths. (a) Depth slice at 6 km indicating relative shear-wave velocity perturbations as dV_S (%) from the average at that depth, with the seismicity above 6 km plotted on top as colored dots, the same as in Figure 2. (b) Depth slice at 24 km with the seismicity above 24 km plotted on top as colored dots, the same as in Figure 2. Tectonic tremor locations (Wech, 2016) as green dots and the active faults modified (Colpron and Nelson, 2020), indicated by white lines, and the epicenter of the 2002 M_w 7.9 Denali fault earthquake shown as a yellow star. The dark red volcanoes indicate the position of the Buzzard Creek (BC) and Jumbo Dome (JD) volcanoes that last erupted in 1050 B.C.E. (Wood and Kienle, 1990). HCF, Hines Creek fault; MD, Mt. Drum; MRVF, Maclaren River volcanic field; SGF, Susitna glacier fault; TF, Talkeetna fault.

interpret the fast seismic velocities to represent cold North American crust above the slab and the low-velocity zones to the east of A–A′ to represent a warmer region where the slab is absent. These interpretations of crustal thermal structure are supported by the presence of volcanic centers in the region characterized by slower (negative) *S*-wave velocity anomalies east of the A–A′ profile and absence of volcanic centers in the region characterized by faster (positive) *S*-wave velocity anomalies to the west (Fig. 4). The projection of this cluster of events also connects the westernmost Wrangell Volcano, Mt Drum, and the active volcanoes on the north flank of the Alaska Range, Buzzard Creek and Jumbo Dome along with the Maclaren River volcanic field (Brueseke *et al.*, 2023), which are outside of the Denali volcanic gap (Figs. 1, 2, and 4). All these observables indicate that the edge of the subducted Yakutat slab is farther east than many prior studies have suggested (Eberhart-Phillips *et al.*, 2006; Miller *et al.*, 2018), although others (e.g., Bauer *et al.*, 2014; Wech, 2016) have suggested that it extends to the Wrangell volcanic field. Considering the new data documenting the lateral extent of the subducted Yakutat microplate presented here, we propose that the Quaternary onset of volcanic fields around the northern and northeastern margins of the imaged Yakutat slab record re-establishment of a mantle wedge since ~ 1 Ma.

ML and inclusion of data from temporary networks reveal the connection between structures in the congested subduction zone of southern Alaska. The newly defined linear trend of small-magnitude earthquakes discovered with the new catalog is collocated with the eastern limit of tectonic tremor (Wech, 2016) and high-*S*-wave velocities in the lower crust of the North American plate, which is thus interpreted to define the edge of the subducted Yakutat slab ~100 km east of the well-defined Wadati–Benioff zone seismicity (Fig. 2a,c), as shown in Figure S3B. The spatial gap between the Wadati–Benioff zone earthquakes and the linear earthquake cluster is filled with tectonic tremor, which may be indicative of sliding of the Yakutat microplate beneath North America in a weak-fault environment with very low effective stress (Wech, 2016). Yet, at the eastern edge of the subducted Yakutat slab, thousands of small earthquakes reappear in a long, dipping line, suggesting a different mechanism of deformation and a change in stress state where the fault strength transitions from

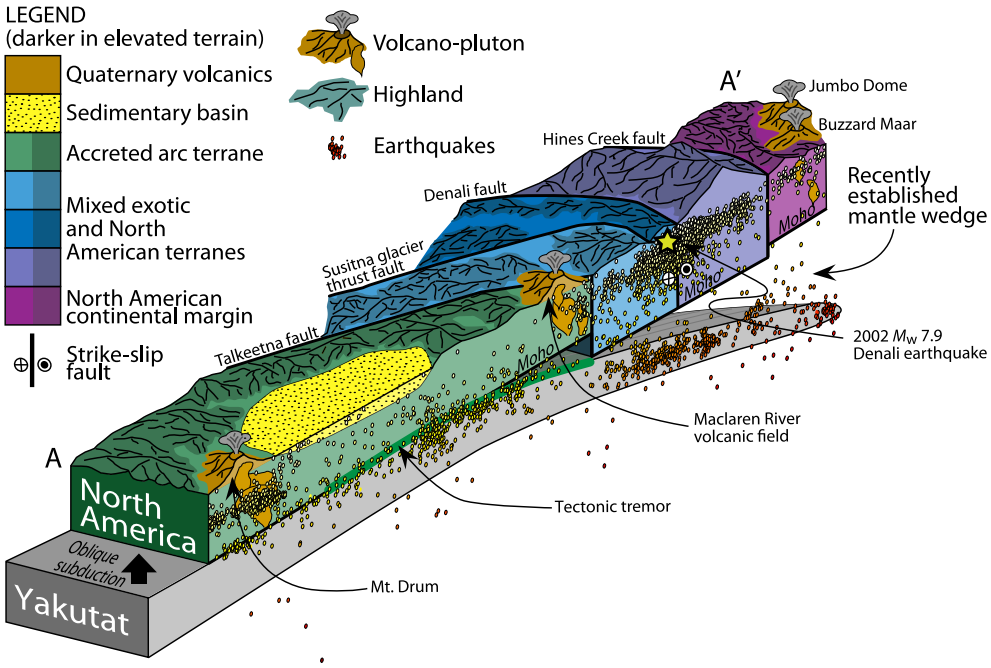

Figure 5. 3D schematic illustrating the tectonic interpretation. Interpretation of the newly defined edge of the Yakutat plate along profile A–A′ (as shown in Figs. 2b and 3a).

continuous, aseismic slip (tremor) back to stick-slip type earthquakes. The linear cluster of earthquakes also intersects the Denali fault at the apex of curvature in the Alaska Range orogen—collocated with the M_w 7.9 Denali earthquake epicenter (Figs. 2 and 5). This razor-sharp line is the locus of changing slab morphology as it cuts through the lithosphere, controlling the location of seismicity in the overriding plate, the shape of the Alaska Range orogen, and the re-establishment of arc volcanoes along the Yakutat slab edge.

Data and Resources

The broadband waveform data can be downloaded from the EarthScope Consortium Data Management Center (http://www.earthscope.org/data) with the network codes (with DOIs) listed in Table S1. The facilities of the EarthScope Data Management Center (https://ds.iris.edu/ds/nodes/dmc) were used for access to waveform and metadata used in this study. The machine learning (ML) catalog is available at AusPass (https://auspass.edu.au/research/catalogs.html) as a bulletin as well as QuakeML. The ambient noise tomography model is available as an EMC Earth Model (doi: 10.17611/dp/emc.2026.alaskaantcrustvs.1). The ML-based code for earthquake catalog building is available at https://github.com/smousavi05/EQTransformer, the associator can be accessed at https://github.com/Dal-mzhang/REAL, and the locator can be accessed here: https://github.com/ut-beg-texnet/NonLinLoc. The ambient noise data processing and dispersion measurement code used in this study is available at https://github.com/fmagrini/seislib. The tomographic inversion code used in this study is available at https://github.com/HongjianFang/DSurfTomo. The receiver function code used in this study is available at https://github.com/rwporritt/funclab. All websites were last accessed in May 2026. Details about the seismic networks, data, methodology, parameters, and tests of our results are documented in the supplemental material.

Declaration of Competing Interests

The authors acknowledge that there are no conflicts of interest recorded.

Acknowledgments

National Science Foundation Award Number EAR-1828737 (S. M. R., T. S. W., and M. S. M.). Australian Research Council grant DP150102887 (M. S. M.).

References

Axen, G. J., J. W. van Wijk, and C. A. Currie (2018). Basal continental mantle lithosphere displaced by flat-slab subduction, *Nat. Geo.* **11,** 961–964.

Bauer, M. A., G. L. Pavlis, and M. Landes (2014). Subduction geometry of the Yakutat terrane, southeastern Alaska, *Geosphere* **10,** 1161–1176.

Brueseke, M. E., J. A. Benowitz, A. T. Bearden, M. E. Mann, and D. P. Miggins (2023). Subduction disruption, slab tears: CA. 1 Ma true collision of an ~30-km-thick oceanic plateau segment recorded by Yakutat slab nascent tear magmatism, *Terra Nova* **35,** 49–57.

Brueseke, M. E., J. A. Benowitz, J. M. Trop, K. N. Davis, S. E. Berkelhammer, P. W. Layer, and B. K. Morter (2019). The Alaska Wrangell Arc: ~30 Ma of subduction-related magmatism along a still active arc-transform junction, *Terra Nova* **31,** 59–66.

Christeson, G. L., H. J. A. Van Avendonk, S. P. S. Gulick, R. S. Reece, G. L. Pavlis, and T. L. Pavlis (2013). Moho interface beneath

Yakutat terrane, southern Alaska, *J. Geophys. Res. Solid Earth* **118,** 5084–5097.

Chuang, L., M. Bostock, A. Wech, and A. Plourde (2017). Plateau subduction, intraslab seismicity, and the Denali (Alaska) volcanic gap, *Geology* **45,** 647–650.

Colpron, M., and J. Nelson (2020). *A Digital Atlas of Terranes for the Northern Cordillera*, Yukon Geological Survey, Whitehorse, Canada.

Crone, A. J., S. F. Personius, P. A. Craw, P. J. Haeussler, and L. A. Staft (2004). The Susitna glacier thrust fault: Characteristics of surface ruptures on the fault that initiated the 2002 Denali fault earthquake, *Bull. Seismol. Soc. Am.* **94,** S5–S22.

Daly, K. A., G. A. Abers, M. E. Mann, S. Roecker, and D. H. Christensen (2021). Subduction of an oceanic plateau across southcentral Alaska: High-resolution seismicity, *J. Geophys. Res. Solid Earth* **126,** e2021JB022809, doi: 10.1029/2021JB022809.

Eberhart-Phillips, D., D. H. Christensen, T. M. Brocher, R. Hansen, N. A. Ruppert, P. J. Haeussler, and G. A. Abers (2006). Imaging the transition from Aleutian subduction to Yakutat collision in central Alaska, with local earthquakes and active source data, *J. Geophys. Res. Solid Earth* **111,** doi: 10.1029/2005JB004240.

Eberhart-Phillips, D., P. J. Haeussler, J. T. Freymueller, A. D. Frankel, C. M. Rubin, P. Craw, N. A. Ratchkovski, G. Anderson, G. A. Carver, A. J. Crone, *et al.* (2003). The 2002 Denali fault earthquake, Alaska: A large magnitude, slip-partitioned event, *Science* **300,** 1113–1118.

Fang, H., H. Yao, H. Zhang, Y.-C. Huang, and R. D. van der Hilst (2015). Direct inversion of surface wave dispersion for three-dimensional shallow crustal structure based on ray tracing: Methodology and application, *Geophys. J. Int.* **201,** 1251–1263.

Ferris, A., G. A. Abers, D. H. Christensen, and E. Veenstra (2003). High resolution image of the subducted Pacific (?) plate beneath central Alaska, 50–150 km depth, *Earth Planet. Sci. Lett.* **214,** 575–588.

Finzel, E. S., L. M. Flesch, K. D. Ridgway, W. E. Holt, and A. Ghosh (2015). Surface motions and intraplate continental deformation in Alaska driven by mantle flow, *Geophys. Res. Lett.* **42,** 4350–4358.

Fuis, G. S., T. E. Moore, G. Plafker, T. M. Brocher, M. A. Fisher, W. D. Mooney, W. J. Nokleberg, R. A. Page, B. C. Beaudoin, N. I. Christensen, *et al.* (2008). Trans-Alaska Crustal Transect and continental evolution involving subduction underplating and synchronous foreland thrusting, *Geology* **36,** 267–270.

Kennett, B. L. N., E. R. Engdahl, and R. Buland (1995). Constraints on seismic velocities in the Earth from travel times, *Geophys. J. Int.* **122,** 108–124.

Magrini, F., S. Lauro, E. Kästle, and L. Boschi (2022). Surface-wave tomography using SeisLib: A Python package for multiscale seismic imaging, *Geophys. J. Int.* **231,** 1011–1030.

Mann, M. E., G. A. Abers, K. A. Daly, and D. H. Christensen (2022). Subduction of an oceanic plateau across southcentral Alaska: Scattered-wave imaging, *J. Geophys. Res. Solid Earth* **127,** e2021JB022697, doi: 10.1029/2021JB022697.

Miller, M. S., L. J. O'Driscoll, R. W. Porritt, and S. M. Roeske (2018). Multiscale crustal architecture of Alaska inferred from P receiver functions, *Lithosphere* **10,** 267–278.

Moresi, L., P. G. Betts, M. S. Miller, and R. A. Cayley (2014). Dynamics of continental accretion, *Nature* **508,** 245–248.

Mousavi, S. M., W. L. Ellsworth, W. Zhu, L. Y. Chuang, and G. C. Beroza (2020). Earthquake transformer—An attentive deep-learning model for simultaneous earthquake detection and phase picking, *Nat. Commun.* **11,** 3952.

Nayak, A., D. Eberhart-Phillips, N. A. Ruppert, H. Fang, M. M. Moore, C. Tape, D. H. Christensen, G. A. Abers, and C. H. Thurber (2020). 3D Seismic Velocity Models for Alaska from joint tomographic inversion of body-wave and surface-wave data, *Seismol. Res. Lett.* **91,** 3106–3119.

Nye, C. (1999). The Denali volcanic gap—Magmatism at the eastern end of the Aleutian arc, *Eos Trans. AGU* **80,** F1202.

Plafker, G., H. C. Berg and , and Geological Society of America (1994). The geology of Alaska, in *The geology of North America v G-1*, Geological Society of America, Boulder, Colorado, 1 online resource pp. 1055.

Porritt, R. W., and M. S. Miller (2018). Updates to FuncLab, a Matlab based GUI for handling receiver functions, *Comput. Geosci.* **111,** 260–271.

Ratchkovski, N. A., S. Wiemer, and R. A. Hansen (2004). Seismotectonics of the Central Denali fault, Alaska, and the 2002 Denali fault Earthquake Sequence, *Bull. Seismol. Soc. Am.* **94,** S156–S174.

Redfield, T. F., D. W. Scholl, P. G. Fitzgerald, and M. E. Beck Jr. (2007). Escape tectonics and the extrusion of Alaska: Past, present, and future, *Geology* **35,** 1039–1042, doi: 10.1130/g23799a.1.

Regan, S. P., J. A. Benowitz, T. S. Waldien, M. E. Holland, S. M. Roeske, P. O'Sullivan, and P. Layer (2021). Long distance plutonic relationships demonstrate 33 million years of strain partitioning along the Denali fault, *Terra Nova* **33,** 630–640.

Rondenay, S., L. G. Montési, and G. A. Abers (2010). New geophysical insight into the origin of the Denali volcanic gap, *Geophys. J. Int.* **182,** 613–630.

Ruppert, N. A., and M. E. West (2019). The Impact of USArray on earthquake monitoring in Alaska, *Seismo. Res. Lett.* **91,** 601–610.

Vallage, A., M. H. Devès, Y. Klinger, G. C. P. King, and N. A. Ruppert (2014). Localized slip and distributed deformation in oblique settings: The example of the Denali fault system, Alaska, *Geophys. J. Int.* **197,** 1284–1298.

Waldien, T. S., M. S. Miller, and S. M. Roeske (2024). Geologic evolution of the Denali fault system and associated crustal structure, in *Tectonics and Seismic Structure of Alaska and Northwestern Canada*, N. A. Ruppert, M. A. Jadamec, and J. T. Freymueller (Editors), American Geophysical Union, Washington, D.C., 547–574.

Wech, A. G. (2016). Extending Alaska's plate boundary: Tectonic tremor generated by Yakutat subduction, *Geology* **44,** 587–590.

Wood, C. A., and J. Kienle (1990). *Volcanoes of North America: United States and Canada*, Cambridge University Press, New York.

Worthington, L. L., H. J. A. Van Avendonk, S. P. S. Gulick, G. L. Christeson, and T. L. Pavlis (2012). Crustal structure of the Yakutat terrane and the evolution of subduction and collision in southern Alaska, *J. Geophys. Res. Solid Earth* **117,** doi: 10.1029/2011JB008493.

Manuscript received 8 December 2025
Published online 4 June 2026